






The Viscosity Parameter for Late-type Stable Be Stars

A. Granada^{1,2} , C. E. Jones³ , and T. A. A. Sigut^{3,4} ¹ Universidad Nacional de Río Negro, Sede Andina, CITECCA, Anasagasti 1461, S.C. de Bariloche, Argentina; agranada@unrn.edu.ar² Consejo Nacional de Investigaciones Científicas y Técnicas, Argentina³ Department of Physics and Astronomy, The University of Western Ontario, London, ON N6A 3K7, Canada⁴ Institute for Earth and Space Exploration (IESX), The University of Western Ontario, London, ON N6A 3K7, Canada

Received 2021 March 5; revised 2021 August 25; accepted 2021 August 26; published 2021 November 26

Abstract

Using hydrodynamic principles we investigate the nature of the disk viscosity following the parameterization by Shakura & Sunyaev adopted for the viscous decretion model in classical Be stars. We consider a radial viscosity distribution including a constant value, a radially variable α assuming a power-law density distribution, and isothermal disks, for a late-B central star. We also extend our analysis by determining a self-consistent temperature disk distribution to model the late-type Be star 1 Delphini, which is thought to have a nonvariable, stable disk as evidenced by H α emission profiles that have remained relatively unchanged for decades. Using standard angular momentum loss rates given by Granada et al., we find values of α of approximately 0.3. Adopting lower values of angular momentum loss rates, i.e., smaller mass loss rates, leads to smaller values of α . The values for α vary smoothly over the H α emitting region and exhibit the biggest variations nearest the central star within about five stellar radii for the late-type, stable Be stars.

Unified Astronomy Thesaurus concepts: [Be stars \(142\)](#); [Circumstellar disks \(235\)](#); [Stellar mass loss \(1613\)](#)

1. Introduction

More than 80 years ago, Struve (1931) noticed that rapid rotation seemed to be a prerequisite to the appearance of bright lines in the spectra of some early-type stars, now known as Be stars, that exhibited broad photospheric lines and bright emission lines. He also pointed out that due to their rapid rotation these objects were likely to lose material at the equator creating a flattened circumstellar shell, where the emission lines form. However, during the decades that followed, the nature and mechanisms involved in the formation of such an envelope were largely debated (as stated in numerous reviews Slettebak 1982; Porter & Rivinius 2003; Rivinius et al. 2013). It is therefore not surprising that even today the most broadly accepted definition of Be stars as being nonsupergiant stars that exhibit, or have exhibited at some time, hydrogen lines in emission (Jaschek et al. 1981) was established on a purely observational basis. For a detailed description of Be star characteristics, we refer the reader to two complete reviews on the subject: Porter & Rivinius (2003) and Rivinius et al. (2013).

During the past two decades, the viscous decretion disk model (VDD; Lee et al. 1991; Okazaki 2001) has become the most successful model to describe a number of the observed characteristics of Be stars, including their variability timescales (Carciofi et al. 2012; Ghoreyshi & Carciofi 2017; Vieira et al. 2017). In the VDD model, the central star loses mass and angular momentum continuously, putting material in a Keplerian orbit at the base of the disk. Beyond this inner boundary, some kind of turbulent viscosity transports the material outwards. If the angular momentum input from the central star is suppressed, the star can lose its disk until a new mass and angular momentum loss regime is set up.

In light of all the new observational data for Be stars, and the success of the VDD model in describing them, Rivinius et al. (2013) suggested to redefine Be stars as rapidly rotating, nonradially pulsating stars without large-scale magnetic fields, that form a VDD in Keplerian rotation around them from the material ejected from the central star.

Despite the success of the VDD model in describing different observables of Be stars, there are still missing pieces to fully understand the appearance of the Be phenomenon. One of these issues is the nature of the viscous mechanism driving the angular momentum throughout the disk.

The kinematic viscosity associated with the mechanism responsible for the transfer of angular momentum outward in a decretion disk is described following the α -parameterization that has been long used to characterize the viscous mechanism of the transfer of angular momentum within accretion disks (Shakura & Sunyaev 1973; Pringle 1981). The viscosity, ν , is written in terms of the local characteristic length (scale height, $H(r)$) and velocity (speed of sound, $c_s(r)$) via $\nu(r) = \alpha H(r)c_s(r)$.

Because of the viscous nature of the circumstellar disk surrounding Be stars, most of what is known about the viscosity comes from the analysis of buildup and destruction phases, which correspond to epochs of changes in the mass loss and/or angular momentum loss rates (Carciofi et al. 2012; Haubois et al. 2014). In most cases, α is assumed to be constant throughout the disk and in time.

In the present work, we propose to obtain information of the viscosity of circumstellar disks surrounding Be stars that have reached a stable state.

We seek to understand whether considering α to be constant throughout the disk of a stable late-type Be star is a good approximation or not, by quantifying how α changes throughout the H α forming region. We note that H α is thought to form in the inner part of the disk out to a radius of order 10 stellar radii (for example, see the reviews by Miroshnichenko et al. 2003 and Rivinius et al. 2013). The actual H α emitting size depends mainly on disk density so there is variation. Of course, the stellar parameters also play a role since the star is the main source of energy to the disk through its ionizing radiation.

We have chosen to focus on rapidly rotating late-type Be stars with stable disks. Even though there is still an open debate on how close to critical Be stars rotate, it has been found that for late Be stars as a group, the rotational velocities are closer to

critical than for early Be stars (Cranmer 2005; Huang et al. 2010). For some (still not understood) reason, the forces involved in the appearance of the Be phenomenon seem to be weaker for these objects, so larger rotational rates would be required in order to launch stellar material into a Keplerian orbit and form a circumstellar disk. This may be the reason why later spectral types, rapidly rotating stars that have never exhibited hydrogen emission lines yet, Bn stars, are most common (Zorec et al. 2007; Cochetti et al. 2020).

For some late-type Be stars the hydrogen emission lines have remained unchanged since the first observations were obtained almost a century ago, evidence that the disk may have had a constant input of matter and angular momentum throughout all this time (see, for example, Merrill 1952; Marlborough & Cowley 1974, for an older description of stable Be stars).

Based on the abovementioned observational pieces of evidence, we propose that late-type Be stars with stable disks are ideal laboratories to study the physics of decretion disks. Moreover, we assume that a series of important simplifications can be made:

1. We assume the central star is rotating at the critical limit and that stellar evolution models adequately describe the required angular momentum loss rates when this occurs.
2. The effects of stellar winds in removing mass and angular momentum from the central star are negligible so the angular momentum is only removed *mechanically* from the equatorial regions of the star.
3. The matter and angular momentum expelled by the central star form a circumstellar disk that is thin, in Keplerian rotation, and has reached a steady state.
4. The angular momentum is transported throughout the disk via a viscous process.
5. We assume the density and thermal distribution for such a disk can be derived from observations.

The paper is organized as follows. In Section 2, we briefly revisit equations to describe the radial viscosity distribution under the assumptions described above. Section 3 considers $\alpha(r)$ for disks with a constant α and a radial variable α assuming power-law density distribution for isothermal disks. We also briefly discuss the viscous timescale and the potential of magnetorotational instabilities to transport angular momentum within the disk. In Section 4, we extend our analysis by including a self-consistent disk temperature distribution to the late-type, stable Be star, 1 Delphini constrained by the observed H α emission profile and spectral energy distribution (SED). A summary and a discussion of our findings are presented in Section 5.

2. The Radial Viscosity Distribution

We briefly recall the treatment of the equation of conservation of angular momentum in an axisymmetric disk in steady state.

Under the assumptions described in the previous section, at each radius r , the viscous torque T exerted on an annulus of a disk is

$$T = 2\pi r^3 \nu \Sigma \frac{d\Omega}{dr}, \quad (1)$$

where $\Sigma(r)$ is the surface density, $\nu(r)$ is the kinematic viscosity, and $\Omega(r)$ is the angular velocity of the annulus. We

note that we adopt italic T for torque and roman T for temperature throughout this article.

Replacing (1) in the vertically integrated azimuthal component of the equation of conservation of angular momentum we have

$$r \frac{\partial}{\partial t} (r^2 \Omega \Sigma) + \frac{\partial}{\partial r} (r^2 \Omega r \Sigma \nu_r) = \frac{1}{2\pi} \frac{\partial T}{\partial r}. \quad (2)$$

In steady state, Equation (2) transforms into

$$\frac{\partial}{\partial r} (r \nu_r \Sigma r^2 \Omega) = \frac{\partial}{\partial r} \left(\nu \Sigma r^3 \frac{\partial \Omega}{\partial r} \right). \quad (3)$$

Integrating,

$$\Sigma \nu_r \Omega = \nu \Sigma \frac{\partial \Omega}{\partial r} + \frac{C}{2\pi r^3}. \quad (4)$$

We should bare in mind that in a viscous disk the surface density depends on the disk viscosity: if the viscous eddies had velocities close to the local speed of sound, shock heating would occur modifying the thermal structure of the disk, and therefore the scale height and the surface density. Because there is no evidence of such shock heating in Be star disks, in the present work we neglect its effects. The fact that radiative processes dominate the disk energy balance in Be star disks has been noted in the literature (for example, see Section 3 in Millar & Marlborough 1998 and references therein). More recently, Kurfürst et al. (2017) found that for $\dot{M} < 10^{-10} M_\odot \text{ yr}^{-1}$, which is satisfied for the present equatorial mass loss rates considered, the effect of viscous heating would be insignificant in Be star disks.

In a decretion disk, the constant C in Equation 4 is the angular momentum loss rate $\dot{\mathcal{L}}$ at the outer boundary of the viscous disk, $C = \dot{\mathcal{L}} = \dot{M} R_{\text{out}}^2 \Omega_{\text{out}}$. The outer radius, R_{out} , is defined as the region where viscosity is no longer efficient in transferring angular momentum (see Krtićka et al. 2011). It is assumed that the mass and angular momentum are supplied at the inner boundary by the critically rotating star. From the equation of continuity,

$$\nu_r = \frac{\dot{M}}{2\pi r \Sigma} = \frac{\dot{\mathcal{L}} / (R_{\text{out}}^2 \Omega_{\text{out}})}{2\pi r \Sigma}. \quad (5)$$

Replacing ν_r in Equation (4) leads to an expression for the viscous torque exerted inside-out at radius r , or equivalently, the flux of angular momentum across a radius r in the disk,

$$T(r) = \dot{M} (r^2 \Omega - R_{\text{out}}^2 \Omega_{\text{out}}), \quad (6)$$

written in terms of the mass loss rate through the viscous disk, \dot{M} , and the difference in specific angular momentum at a radius r and at the outer border of the disk. Replacing $T(r)$ with Equation 1 gives us the radial dependence of the kinematic viscosity,

$$\nu(r) = \frac{\dot{M}}{\Sigma \frac{\partial \Omega}{\partial r} 2\pi r^3} (r^2 \Omega - R_{\text{out}}^2 \Omega_{\text{out}}). \quad (7)$$

Following the numerical calculations by Krtićka et al. (2011; and also Kurfürst et al. 2014), $\Omega_{\text{out}} R_{\text{out}}^2 = 0.5 \sqrt{GMR_{\text{out}}}$. As shown by these authors, between the stellar surface and the outer disk radius, $\Omega r^2 = \kappa(r) \sqrt{GMr}$. Close to the central star within the innermost 80 stellar radii, which largely covers the forming region of traditional disk tracers as the H α line, we can

assume that $\kappa(r) = 1$, which means that the disk is in Keplerian rotation. In this work, we will consider we are close enough to the star so that this assumption is valid. In this case, we can rewrite Equation 7 as,

$$\nu(r) = \frac{\dot{M}}{3\pi\Sigma} \left(\frac{1}{2} \sqrt{\frac{R_{\text{out}}}{r}} - 1 \right). \quad (8)$$

We also consider for the present analysis that r is significantly smaller than $R_{\text{out}}/4$ so that the term between brackets is always positive in our analysis. Then, if we consider the mass loss rate from evolutionary models and the surface density of the viscous Keplerian disk derived from observations, we can investigate the radial dependency of the viscosity that is compatible with such a disk structure.

We are implicitly assuming here that the density structures derived from observations are the result of the viscous mechanism driving the disk.

In this sense, we describe how the viscosity parameter, α , changes with radial distance relating the viscosity to $H(r)$ and velocity, $c_s(r)$. Under the assumption that the disk is isothermal in the vertical direction, we can write the speed of sound as $c_s(r) = \sqrt{(kT(r))/(\mu m_H)}$, where k is Boltzmann's constant, μ the mean molecular weight, and m_H the mass of the hydrogen atom. In the case in which the vertical structure of the disk is not considered isothermal, we define the characteristic speed of sound by replacing $T(r)$ by the density weighted temperature (see Equation (11) in Sicut et al. 2009 and Section 4). We then obtain,

$$\alpha(r) = \frac{\nu(r)}{H(r)c_s(r)}. \quad (9)$$

It is worth pointing out that there is a dependence between the disk temperature distribution and the value of the viscosity via the sound speed.

3. $\alpha(r)$ for Particular Cases

As mentioned in the previous section, throughout the present work we assume that the mechanical angular momentum loss rate, $\dot{\mathcal{L}}$, is supplied by a critically rotating central star. This quantity can be obtained from stellar evolution calculations using the Geneva code (Ekström et al. 2012; Georgy et al. 2013). Then, in order to derive an estimate for \dot{M} , we use the expression provided by Krtićka et al. (2011) that takes into account that at large distances from the star, the disk is no longer rotating with Keplerian velocities. These authors showed that the angular momentum loss rate $\dot{\mathcal{L}}$ at the outer radius and the mass loss rate are related via,

$$\dot{\mathcal{L}} = \frac{1}{2} \dot{M} V_K(R_{\text{out}}) R_{\text{out}}, \quad (10)$$

with the outer radius given by

$$\frac{R_{\text{out}}}{R_o} = \left[\frac{3}{10 + 4m} \left(\frac{V_{KR_o}}{c_{sR_o}} \right)^2 \right]^{\frac{1}{1-m}}, \quad (11)$$

with R_o being the stellar equatorial radius, and V_{KR_o} and c_{sR_o} being the Keplerian velocity and speed of sound at the stellar equator, respectively. Here, we are assuming that the disk is not truncated by an orbiting companion and, therefore, this expression is likely an upper limit for $\dot{\mathcal{L}}$. As described in

more detail later, the parameter, m , is the exponent when considering a power-law temperature distribution.

Using these relations, Granada et al. (2013) provided values for mean mechanical angular momentum loss rates, the corresponding disk outer radius and mass loss rates for stars between 1.7 and 15 M_\odot , and different metallicities, assuming an isothermal disk. Considering $\alpha = 1$, viscous timescales and disk masses were also derived.

Because the outer radius, and hence the mass loss rate, do not strongly depend on the viscosity parameter α throughout the disk, we use the previous expressions even in the case of a radially varying α .

3.1. The Particular Case of a Disk with Radially Constant α

As is usually done in the literature, for example, see Carciofi (2011), we first consider the case of α being constant throughout the vertically isothermal disk. In this case, replacing $\nu = \alpha c_s(r)H(r) = \alpha c_s(r)^2/\Omega(r)$, and considering once again that $\Omega(r)$ is the Keplerian angular velocity, the known expression for the surface density $\Sigma(r)$ is obtained:

$$\Sigma(r) = \frac{\dot{M}\Omega_o}{3\pi\alpha} \left(\frac{R_o}{R_{\text{out}}} \right)^{\frac{3}{2}} \frac{1}{c_s^2} \left(\frac{R_{\text{out}}}{r} \right)^{\frac{3}{2}} \left(\frac{1}{2} \sqrt{\frac{R_{\text{out}}}{r}} - 1 \right). \quad (12)$$

This relation shows that close to the star the surface density $\Sigma(r) \propto r^{-2}$ if the disk is isothermal, or equivalently $\rho(r) \propto r^{-3.5}$. As before, the subscript o indicates quantities at the equatorial radius. We note that in what follows we often describe density distribution with a base value of ρ_o at the innermost part of the disk at the stellar surface in the equatorial region, which falls off with a power-law value denoted by n .

If we evaluate the previous equation at $r = R_o$ and rearrange the terms, we have an expression for α , constant throughout the disk:

$$\alpha = \frac{\dot{M}\Omega_o}{3\pi\sigma c_{sR_o}^2} \left(\frac{1}{2} \sqrt{\frac{R_{\text{out}}}{R_o}} - 1 \right). \quad (13)$$

We can derive the mass loss rates through the angular momentum loss rates obtained from stellar evolution calculations directly from Table 5 in Granada et al. (2013) and the outer disk radius computed using the expression given by Krtićka et al. (2011). These mass loss rates are therefore independent of α . We note that during the mechanical mass loss phase, the star is assumed to be rotating critically with the T_{eff} consistent with the stellar luminosity and surface of the rotationally distorted star. Considering also a base density of $\rho_o = 10^{-11} \text{ g cm}^{-3}$ and an isothermal disk temperature (T_d) of 0.6 T_{eff} (Carciofi & Bjorkman 2006), typical values derived from the observation of steady state disks surrounding Be stars (Rivinius et al. 2013 and references therein), we find that α is 0.136, 0.365, and 0.422 for stars of 3, 4, and 5 M_\odot , respectively. If instead of considering the same value of ρ_o , we assumed a mass dependent value for ρ_o of $3 \times 10^{-12} \text{ g cm}^{-3}$, $8 \times 10^{-12} \text{ g cm}^{-3}$, and $10^{-11} \text{ g cm}^{-3}$ for 3, 4, and 5 M_\odot stars, the values of α are 0.454, 0.456, and 0.422. Interestingly, these values around 0.5 are between the median values obtained for disk buildup ($\alpha = 0.63$) and disk dissipation phases ($\alpha = 0.26$) by Rímulo et al. (2018).

3.2. Radially Variable α : General Solution for Power-law Dependences

For a disk that is isothermal in the vertical direction, the density law is written as

$$\rho(r, Z) = \rho_0 \left(\frac{r_0}{r} \right)^n e^{-0.5 \left(\frac{Z}{H} \right)^2}, \quad (14)$$

with the scaleheight

$$H(r) = H_0 \left(\frac{r}{r_0} \right)^s, \quad (15)$$

and $H_0 = c_{s0}/\Omega_0$. In this case, the subscript “o,” refers to the innermost grid location of the disk nearest the star in the equatorial plane. The radial power-law dependence, typically assumed for Be star disks, has succeeded in describing different observables during the past decades, with values of n ranging between 2 and 4 (see Rivinius et al. 2013 and references therein).

For a temperature law also following a power law

$$T(r) = T_0 \left(\frac{r}{r_0} \right)^m, \quad (16)$$

the exponent of the power law characterizing the scale height is $s = (3 - m)/2$. In this case

$$\Sigma(r) = \Sigma_0 \left(\frac{r}{r_0} \right)^{\frac{3-m}{2} - n}, \quad (17)$$

where $\Sigma_0 = \sqrt{2\pi} \rho_0 H_0$.

Replacing these relations in Equation 9, we find an expression for the radial dependence for the parameter α ,

$$\alpha(r) = \frac{\dot{M} \Omega_0}{3\pi \Sigma_0 c_{s0}^2} \left(\frac{r}{R_0} \right)^{n + \frac{3}{2}m - 3} \left(\frac{1}{2} \sqrt{\frac{R_{\text{out}}}{r}} - 1 \right). \quad (18)$$

For a certain stellar mass and fixed value of \dot{M} , that is linked to the angular momentum loss rate via $\dot{L} = \dot{M} R_{\text{out}}^2 \Omega_{\text{out}}$, the shape of this curve depends only on the parameters n and m .

3.3. Solution for Isothermal Disks

A particular case of the general power-law dependences is the case of an isothermal Keplerian disk, $m = 0$, which is the model typically used to represent Be disks.

In this case, the exponent s describing radial dependence of the scaleheight is $3/2$ and the speed of sound c_s is constant throughout the disk. Then, Equation (18) results in,

$$\alpha(r) = \frac{\dot{M} \Omega_0}{3\pi \Sigma_0 c_{s0}^2} \left(\frac{r}{R_0} \right)^{n-3} \left(\frac{1}{2} \sqrt{\frac{R_{\text{out}}}{r}} - 1 \right). \quad (19)$$

For fixed values of stellar mass and \dot{M} , the shape of this curve depends only on the parameter n .

We consider again a central star of 3, 4, and $5 M_\odot$ with the corresponding equatorial radius and mean angular momentum loss rate as given by Granada et al. (2013). We assume that the disk isothermal temperature, T_d , is $0.6 T_{\text{eff}}$ and $\rho_0 = 10^{-11} \text{g cm}^{-3}$, for four different values of n , 2.75, 3.25, 3.50, and 3.75. The resulting α distributions are plotted in Figure 1. The innermost values of α lead to small outflow velocities at the inner boundary of the disk, as those listed in Table 1, which are consistent with observations of Be star disks for which no evidence of large outflow velocities are found close to the central star. For values of

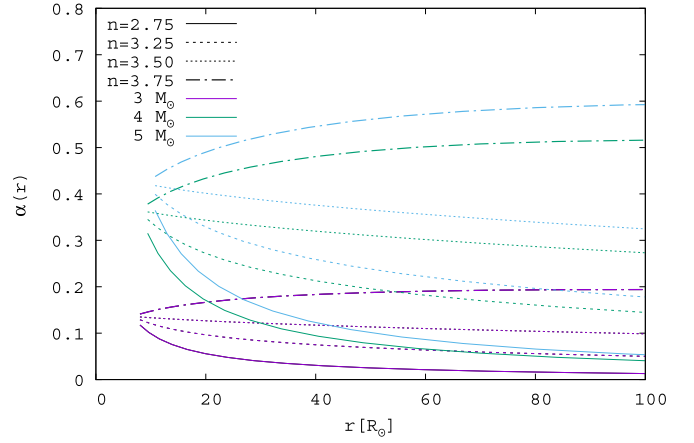


Figure 1. $\alpha(r)$ in the innermost $100 R_\odot$, where the $H\alpha$ line is formed. For $n = 3.5$, $\alpha(r)$ changes little with radius; however, for the other values of n , there are changes in α , most notably in the innermost regions.

$n \leq 3.5$, α decreases for all radii, whereas for values of $n > 3.5$ it increases, reaches a maximum value, and then decreases outwards. We present the value of α at the inner border of the disk (α_0), at 10 stellar radii (α_{10}), and at 20 stellar radii (α_{20}) in Table 1.

We briefly comment on how $\alpha(r)$ behaves when other parameters (other than the mass of the central star and n) are changed.

From Equation (18), it is clear that taking different values for ρ_0 , T_d , and \dot{L} (that changes \dot{M}) does not change the shape of $\alpha(r)$, but simply scales it. Smaller densities and temperatures and larger angular momentum loss rates lead to larger values of α .

Modifying \dot{M} while keeping \dot{L} unchanged is equivalent to changing the outer radius, and this changes the shape of $\alpha(r)$. When R_{out} is decreased by 25% of the standard value, α_0 is slightly smaller, and α decreases faster with radius than the standard case.

In the case in which a nonisothermal disk is considered ($m > 0$ in Equation (18)), the behavior of α is similar to that of an isothermal disk with a larger parameter n , with a different outer radius.

3.4. The Viscous Timescale

Under the mentioned assumptions we can also estimate the viscous timescale that characterizes the disk evolution from the inner radius up to a distance r considering

$$t_{\text{viscous}}(R) = \int_{R_0}^R \left(\frac{2r}{\nu(r)} - \frac{\nu'(r)r^2}{\nu^2(r)} \right) dr. \quad (20)$$

We provide the viscous timescales up to 10 and 20 stellar radii (t_{10} and t_{20} , respectively), representative of the $H\alpha$ line forming region, in Table 1. The tabulated timescales are compatible with the long-term variability observed in late-type Be stars. Through the study of the long-term photometric variability of a few late-type Be stars Hirata (1995) obtained long-term cycles of 10–30 yr, and found these stars spent about 20% of the time in the buildup phase and the rest of the time recovering slowly to their initial state. In this particular study, the sample consisted of Be stars in binary systems. Hubert & Floquet (1998) characterized timescales of variability for Be stars from Hipparcos photometry. They obtained cycles within the Hipparcos mission ($P < 1200$ days) for Be stars earlier than B6 spectral type. Also, similar to Hirata (1995), they found in the case of late Be stars that their light curve varied smoothly,

Table 1
Column 1: Mass of the Central Star

M_* (M_\odot)	v_0 (km s^{-1})	α_0	B_{z0} (G)	n	α_{10}	$t_{\nu 10}$ (yr)	B_{z10} (G)	α_{20}	$t_{\nu 20}$ (yr)	B_{z20} (G)
3	0.004	0.136	6.277	3.75	0.192	8.9	0.086	0.192	15.0	0.023
				3.50	0.108	18.9	0.114	0.091	35.6	0.034
				3.25	0.061	37.2	0.151	0.043	80.4	0.049
				2.75	0.019	133.1	0.268	0.010	391.5	0.103
4	0.011	0.365	7.051	3.75	0.511	3.3	0.096	0.509	5.6	0.026
				3.50	0.288	7.0	0.128	0.241	13.4	0.038
				3.25	0.162	13.9	0.170	0.114	30.2	0.055
				2.75	0.051	26.5	0.226	0.026	66.7	0.080
5	0.015	0.422	7.642	3.75	0.590	2.9	0.104	0.586	5.0	0.028
				3.50	0.332	6.2	0.139	0.277	18.8	0.041
				3.25	0.187	12.2	0.184	0.131	26.7	0.060
				2.75	0.059	43.8	0.326	0.030	129.8	0.126

Note. Columns 2–4, radial velocity, α , and magnetic field at the inner boundary of the disk, respectively. Column 5: value of n characterizing the isothermal models with $\rho_0 = 10^{-11} \text{ g cm}^{-3}$. Columns 6–8, α , viscous timescale, and magnetic field at 10 stellar radii. Columns 9–11, α , viscous timescale, and magnetic field at 20 stellar radii.

Table 2
Same as Table 1 but Considering Values of $\rho_0 = 3 \times 10^{-12} \text{ g cm}^{-3}$ and $\rho_0 = 8 \times 10^{-12} \text{ g cm}^{-3}$ for the $3 M_\odot$ and $4 M_\odot$ Models, Respectively

M_* (M_\odot)	v_0 (km s^{-1})	α_0	B_{z0} (G)	n	α_{10}	$t_{\nu 10}$ (yr)	B_{z10} (G)	α_{20}	$t_{\nu 20}$ (yr)	B_{z20} (G)
3	0.012	0.454	3.438	3.75	0.639	2.7	0.047	0.639	4.5	0.013
				3.50	0.360	5.7	0.062	0.303	10.7	0.019
				3.25	0.203	11.2	0.083	0.143	24.1	0.027
				2.75	0.064	39.9	0.147	0.032	117.4	0.057
4	0.014	0.456	6.306	3.75	0.639	2.7	0.086	0.636	4.5	0.023
				3.50	0.360	5.6	0.114	0.301	10.7	0.034
				3.25	0.203	11.1	0.152	0.143	24.1	0.049
				2.75	0.064	21.2	0.202	0.032	61.5	0.072

not disturbed by short-lived outbursts. In a more recent study, Labadie-Bartz et al. (2018) studied the growth and evolution of circumstellar disks around classical Be stars through the analysis of optical time-series photometry with simultaneous spectroscopy for a sample of 160 Be stars. As in previous works, they found that outbursts are more commonly observed in early (57%), compared to mid- (27%) and late-type (8%) systems, and determined that the average outburst takes about twice as long to dissipate as it does to build up in optical photometry for mid and early Be stars, and probably longer for late Be stars. Our timescales, computed for a typical density at the base of the disk of $10^{-11} \text{ g cm}^{-3}$, are listed in Table 1 and increase for smaller stellar masses, which is consistent with the fact that late Be stars tend to have longer-lasting disks. With the aim of exploring how a change in the base density changes the timescales, we considered smaller values of ρ_0 , $3 \times 10^{-12} \text{ g cm}^{-3}$, and $8 \times 10^{-12} \text{ g cm}^{-3}$, which follows the trend described by Vieira et al. (2017), where smaller base densities are observed for later spectral types. For this set of ρ_0 , the viscous timescales are very similar for the range of masses described in the present work.

3.5. Magnetorotational Instability as the Mechanism Transferring Angular Momentum throughout the Disk

As shown by Krtićka et al. (2015), the magnetorotational instability (MRI; Balbus & Hawley 1991) could be a source of

anomalous viscosity in outflowing disks. Based on an order-of-magnitude viscosity estimate for an isothermal accretion disk, Krtićka et al. (2015) found that α does not depend on the radius close to the star. As shown in Figure 1, we recover a similar behavior for an isothermal disk with $n = 3.5$.

We assume here that MRI is the mechanism driving the angular momentum throughout Be star disks not only for the isothermal case with the density parameter $n = 3.5$, but also for other disk structures. Krtićka et al. (2015) provided a useful expression written in scaled quantities for the strongest vertical equatorial magnetic field B_z that allows the instabilities to develop:

$$B_z < 250 \text{ G} \left[\left(\frac{c_S/v_r}{10^3} \right) v_{K100} \dot{M}_{-9} \right]^{\frac{1}{2}} \left(\frac{r}{R_\odot} \right)^{-1}, \quad (21)$$

where v_{K100} is the rotational velocity at the radius r in units of 100 km s^{-1} and \dot{M}_{-9} is the mass loss rate given in units of $10^{-9} M_\odot \text{ yr}^{-1}$.

Then, for the different isothermal disk structures mentioned in the previous subsection, we computed the maximum vertical component of the magnetic field B_z that allows the instabilities to develop at the inner border of the disk (B_{z0}), and also at 10 and 20 stellar radii (B_{z10} and B_{z20} , respectively). The results are summarized in Tables 1 and 2. We find that in all cases the maximum allowed value B_{z0} is less than 10 G , compatible with

the nondetection of large-scale magnetic fields in Be stars (Wade et al. 2014).

4. A Self-consistent Density and Temperature Distribution: The Disk of the Be-shell Star 1 Delphini

1 Delphini (HD 195325) is a late-type, Be-shell star. The shell star designation follows from the deep central absorption observed in $H\alpha$, indicating that its disk is seen nearly equator-on. 1 Del’s large projected rotational velocity is consistent with a shell star status, with $v \sin i$ values in the literature ranging between 200 and 320 km s^{-1} (Bernacca & Perinotto 1970; Uesugi & Fukuda 1970; Abt & Morrell 1995; Royer et al. 2002). 1 Del may be rotating close to its critical limit, and such an object is expected to be deformed and gravity darkened by rotation. The $H\alpha$ profile of 1 Del has remained virtually unchanged since the first spectra were obtained almost one century ago (Merrill 1952; Marlborough & Cowley 1974; Gulliver 1981; Silaj et al. 2014), with the exception of Iliev & Kubát (2013), Kubát et al. (2016), and Abt (2008), who reported very marginal variations.

The stability of the profile through several decades indicates that there is a constant mass and angular momentum input from the star into the circumstellar disk, making it an excellent target to study disk viscosity as proposed in the previous sections.

We have modeled the $H\alpha$ line profile and near-IR SED of 1 Del using the radiative transfer codes BEDISK (Sigut & Jones 2007; McGill et al. 2011) and BERAY (Sigut 2011). Details of the modeling approach, as applied to the Be-shell star o Aqr, can be found in Sigut et al. (2015), although in the present case we do not have interferometric visibilities. Our computational grid consists of a total of 2600 disk locations including 65 radial positions out to a distance of ~ 200 solar radii with 40 vertical positions at each radial location. The grid is nonuniform to ensure greater sampling nearest the star and in the equatorial plane where density and potentially temperature change more rapidly. Briefly, we have assumed 1 Del is an $M = 3.8 M_{\odot}$ star with a polar radius of $R_p = 3.7$ solar radii rotating at 90% of its critical speed. These stellar parameters are consistent with other values available in the literature for 1 Delphini (e.g., Kervella et al. 2019). In the Roche model, this gives an equatorial-to-polar radius ratio of 1.37 and a polar to equatorial T_{eff} range of 13,150–9460 K, assuming the Espinosa Lara & Rieutord (2011) treatment of gravitational darkening. $H\alpha$ line profiles and near-IR SEDs were computed assuming that the central star is surrounded by an axisymmetric, equatorial, circumstellar disk in Keplerian rotation with a density variation given by Equation (14).

In this equation, we take r_0 to be the star’s equatorial radius, R_{\odot} . The disk scale height, H , was computed assuming the disk is in vertical hydrostatic equilibrium (Sigut et al. 2009), giving $s = 3/2$, i.e., $H \propto r^{3/2}$. Thus the disk density is described by the base density of the disk, ρ_0 , and the power-law index, n . The disk is assumed to extend out to a radius of R_d equatorial radii, and the star-plus-disk system is viewed at an inclination angle (angle between the star’s rotation axis and the line of sight) of i . Thus each computed $H\alpha$ line profile and near-IR SED is a function of the four model parameters (ρ_0 , n , R_d , and i). In the computational pipeline, the BEDISK code computes the thermal structure of the disk, $T(R, Z)$, by enforcing radiative equilibrium in a gas of solar composition, and the BERAY code solves the radiative transfer equation along a series of rays directed at the observer. Rays that terminate on the stellar

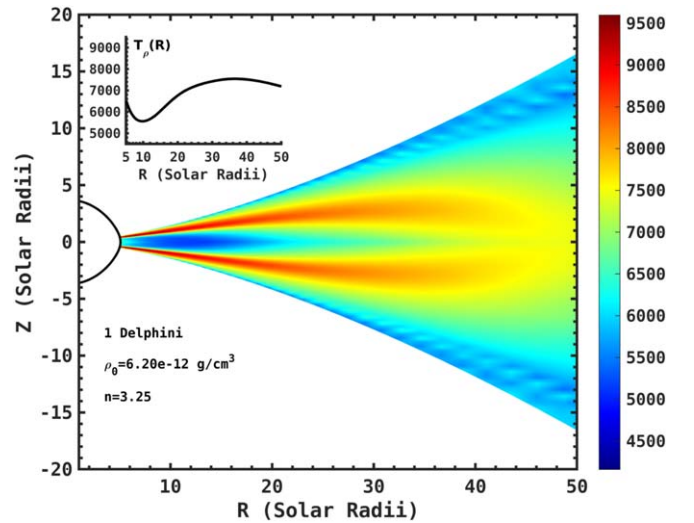


Figure 2. Disk temperatures, $T(R, Z)$ in Kelvin, for the model with $\rho_0 = 6.2 \times 10^{-12} \text{ g cm}^{-3}$ and $n = 3.25$. The stellar outline is indicated. The upper left insert shows the density weighted disk temperature as a function of disk radius.

surface use an appropriately Doppler-shifted, LTE, photospheric $H\alpha$ line or photospheric continuum intensity (based on the local, stellar surface value of T_{eff} and $\log g$ where the ray terminates) for the intensity boundary condition on the transfer equation.

Figure 2 shows our calculated disk temperature distribution through a slice of the disk as a function of radial distance and height above and below the equatorial plane for the model with $\rho_0 = 6.2 \times 10^{-12} \text{ g cm}^{-3}$ and $n = 3.25$. Note that near the star in the equatorial plane, the optical depths are greater, which results in a region of cooler gas. The upper left of the Figure 2 provides the density weighted temperature as a function of radial distance. We use this average temperature, as explained in detail below, for our $\alpha(r)$ analysis.

$H\alpha$ line profiles and SEDs were computed for disk parameters in the range of $\rho_0 = 1 \times 10^{-12}$ to $2.5 \times 10^{-10} \text{ gm cm}^{-3}$ (19 values equally spaced in $\log_{10} \rho_0$), $n = 1.5$ –4.0 (11 values in equal steps of 0.25), $R_d = 10, 15, 20, 25,$ and $50 R_{\odot}$, and inclinations from $i = 76^{\circ}$ – 88° in steps of 2° . In total, a library of 7315 individual model $H\alpha$ and near-IR SEDs were computed. The best-fit $H\alpha$ profiles were selected as those having the smallest absolute percentage difference between the observed spectrum and model line within the central $\pm 15 \text{ \AA}$ of $H\alpha$. The top five models are shown in Figure 3 along with an observed $H\alpha$ profile of 1 Del originally presented in Silaj et al. (2010; see Table 4) and subsequently modeled in Silaj et al. (2014). The profile is from JD 2454453.5 (2007) and was observed by the 42 inch John S. Hall Telescope at the Lowell Observatory located in Flagstaff, Arizona, with a resolving power of 10,000. The best profile fits all have $i = 84^{\circ}$ with $R_d \geq 20 R_{\text{eq}}$ and $(n, \rho_0) = (2.75, 2.5 \times 10^{-12})$ or $(3.25, 6.2 \times 10^{-12})$ as shown in Figure 3. The residuals between the observed profile and the models are shown at the bottom of the Figure.

Since 1 Del’s disk is observed to be very stable, the $n = 3.25$ solution may be slightly preferred as Vieira et al. (2017) suggest that stable disks are expected to have n in the range of 3.0–3.5; though, different pieces of evidence indicate that stable late-type Be stars seem to prefer values of $n \leq 3$, as is the case for $\beta \text{ CMi}$ with $n = 2.9$ (Klement et al. 2017), and the case of o Aqr with $n = 3$ (de Almeida et al. 2020). Finally, $i = 84^{\circ}$

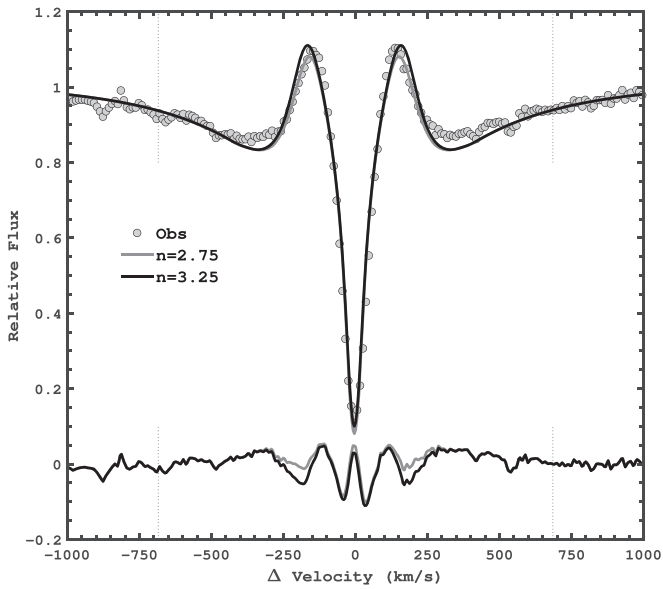


Figure 3. The best-fit profiles to the observed $H\alpha$ profile of 1 Del from Silaj et al. (2014) fall into essentially two groups: one with $n = 2.75$ (two profiles, light gray line) and $n = 3.25$ (three profiles, black line). All models have $i = 84^\circ$. The difference between the model profiles and the observations is shown at the bottom. The vertical dotted lines indicate the wavelength range used in the fitting procedure.

implies $v \sin i = 325 \text{ km s}^{-1}$, which is at the upper limit of suggested values.

We adopted the observed SED of 1 Del from Pickles & Depagne (2010), which specifies the spectrum at 10 wavelengths, from 0.42 to $22.1 \mu\text{m}$. The fluxes for 1 Del were assembled by Pickles & Depagne (2010) using photometric observations from 2MASS, WISE, and AKARI. To compare the observed and model fluxes, the models were normalized to the observed optical flux at $0.42 \mu\text{m}$. However, the issue of reddening must be considered, particularly as the distance to 1 Del is 228 pc . We note that 1 Del’s IR excess is very small or even perhaps has a deficit of IR flux, and there seems to be no information available on a reliable $E(B - V)$ for 1 Del. For this reason, the observed fluxes were dereddened for an $E(B - V)$ ranging from 0 to 0.2 (using the extinction curve of Fitzpatrick (1999) and $A_V/E(B - V) = 3.1$) and compared to the models. Overall, an $E(B - V) = 0.13$ gave the best fit to the SED over all models and $E(B - V)$ values considered. As with the $H\alpha$ line profiles, very good fits to the SED were obtained, as shown in Figure 4.

1 Del’s IR continuum can be matched by a wide range of models with n ranging from $n = 1.5$ to $n = 4.0$. However, the allowed range of parameters does overlap with the previously selected parameters of the $H\alpha$ line profile. The $H\alpha$ line profile is more constraining because of the presence of positional information within the disk provided by the projected surfaces of constant radial velocity on the sky arising from the Keplerian rotation of the disk. For this reason, we adopt the parameters determined from the $H\alpha$ profile matching as the best representatives of 1 Del’s disk density distribution.

Figure 5 shows our best-fit $H\alpha$ profiles and our SED fitting over our computational grid, which we call the disk parameter grid. The $H\alpha$ fits are shown as circles which are increasingly smaller and lighter as the fit figure-of-merit increases. We see that the best fits from $H\alpha$ modeling are along an approximately diagonal position in the Figure. This is expected since with

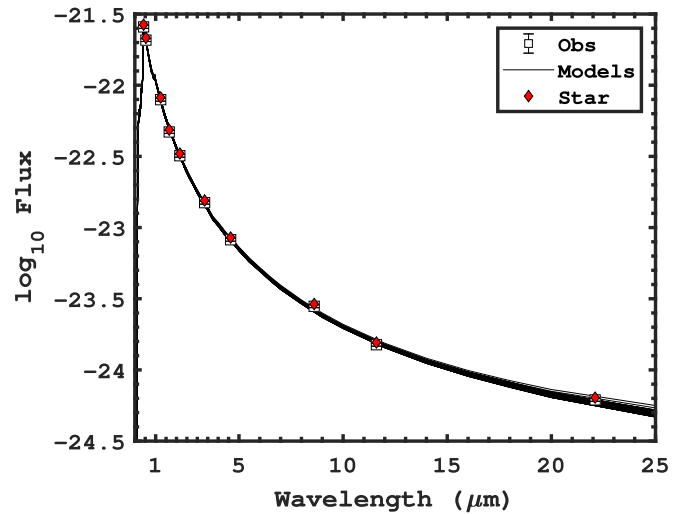


Figure 4. The best-fit models to the observed SED of 1 Del satisfying a reduced $\chi^2 < 1.75$. The best-fitting model has a reduced χ^2 of 1.35. The solid lines are the model fluxes, and the open squares are the observed fluxes normalized to the models at $\lambda = 0.42 \mu\text{m}$ and dereddened assuming $E(B - V) = 0.13$, as discussed in the text. The red diamonds are the predicted model fluxes of the star alone. The errors in observed fluxes are smaller than the symbols. The red diamonds are the predicted fluxes of the star alone (without a disk). Note that the IR excess of 1 Del seems very small or even negative (i.e. with an IR flux deficit).

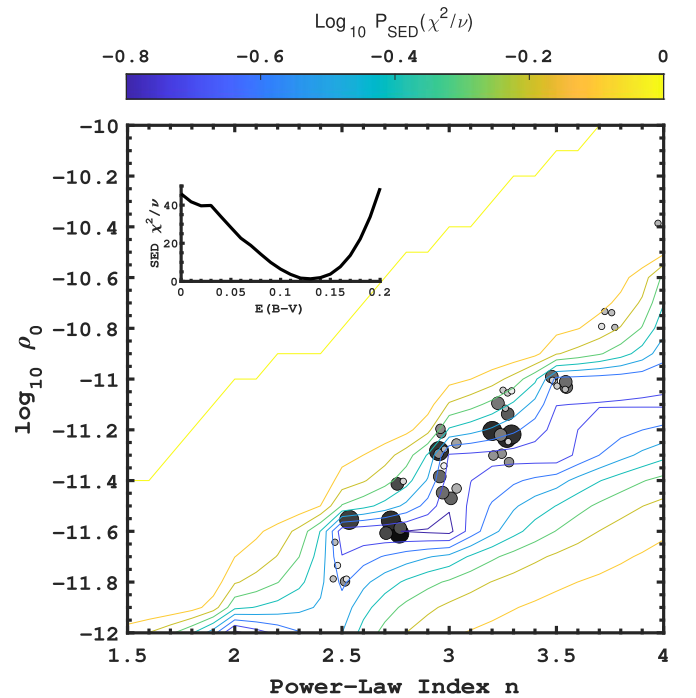


Figure 5. The best-fit models of both $H\alpha$ (symbols) and the SED (contours) in the $(n, \log \rho_0)$ disk parameter plane. The $H\alpha$ profile models are shown as circles, which become smaller and lighter as the figure-of-merit increases. Shown are all $(n, \log \rho_0)$ combinations that fit the $H\alpha$ profile within 25% of the best figure-of-merit. The SED fits are shown as contours of equal $\log P(\chi^2/\nu)$ according to the color bar at the top. The observed SED was dereddened assuming an $E(B - V) = 0.13$. The inset plot shows the reduced χ^2 of the SED fit as a function of the assumed $E(B - V)$, where a strong minimum at $E(B - V) = 0.13$ is seen.

increasing density, ρ , and an increase in the value of n essentially results in a similar overall amount of $H\alpha$ emitting gas. The SED fits are shown as contours corresponding to the

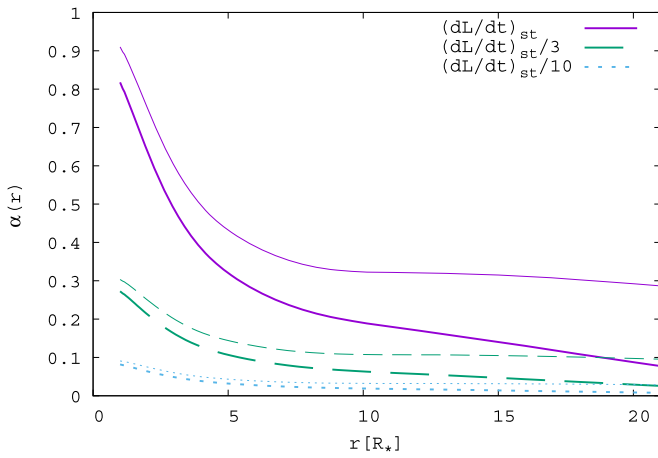


Figure 6. α vs. radial distance in the innermost $20 R_0$. The continuous purple lines correspond to the standard angular momentum loss rate from Granada et al. (2013), the green dashed lines to the standard value divided by 3, and the blue dotted lines to one-tenth of the standard value. The thick lines consider the mass loss rate, \dot{M} , as computed using Equation (15) from Krtićka et al. (2011). The thin lines have \dot{M} divided by two with a corresponding increase in R_d of four.

color bar at the top of the figure. The inset at the top left of the figure shows the reduced χ^2 as a function of $E(B - V)$. Note the minimum, at the location corresponding to $E(B - V) = 0.13$, at the value that corresponds to our best-fitting SED. The reduced χ^2 for our best-fitting SED is 1.35.

In order to explore the $\alpha(r)$ distribution, we use as inputs the disk density profile and the corresponding temperature profile, together with the angular momentum loss rate predicted from stellar evolution models for a star corresponding to the observed spectral type of 1 Del, as obtained in Granada et al. (2013). It is important to remark that to compute $\alpha(r)$ for 1 Del we used the density weighted temperature (Sigut et al. 2009) corresponding to the thermal structure computed by BEDISK for the best fit of $H\alpha$ and the SED. Through this density weighted temperature, we obtained the radial dependence of the sound speed and of the scale height. We also note that for a nonisothermal disk, it is possible to vary $T(r)$ and $\alpha(r)$ in such a way as to keep $\nu(r)$ constant. Therefore, in this case, α and T are degenerate. This issue was examined in detail by Marr et al. (2021) in the case of the Be star, 66 Ophiuchus. However, in our study, this degeneracy is not a factor because we use the temperature structure to calculate $\alpha(r)$.

The results are summarized in Figure 6, which shows α versus radial distance. We chose to show the innermost $20 R_*$ so that the changes in α near the central star can easily be seen. We note that this radial distance is also where the bulk of the $H\alpha$ line profile forms. The thick continuous purple line assumes the angular momentum rate from Granada et al. (2013) and the mass loss rate, \dot{M} , as computed using Equation (15) from Krtićka et al. (2011). These authors showed that the solution actually does not depend significantly on α , but that the temperature structure was important, affecting the disk outer radius and therefore the mass loss rate for a given angular momentum loss rate. Because of this, we explore how $\alpha(r)$ changes for different values of \dot{M} and R_d . Specifically, for the continuous thin purple line, \dot{M} has been divided by two and in order to keep the angular momentum rate fixed, R_d has been increased by four. The thick and thin, dashed green and blue dotted lines use the same scheme as the thick and thin purple lines except that the green dashed lines show $\alpha(r)$ when the

angular momentum loss rate from Granada et al. (2013) is divided by 3, and the blue dotted lines by 10. We chose to explore these smaller values for the angular momentum loss rates because recently smaller values have been suggested in the literature. For example, Rímulo et al. (2018) obtained that the angular momentum rates obtained from Be stellar models seem to be overestimated within an order of magnitude. Alternatively, when considering a fixed value of angular momentum loss rate and density structure, larger values of \dot{M} predict outer radii that are too small (smaller than $r \sim 100 R_0$) and large radial velocities that are not observed, so we do not consider such values.

Figure 6 shows that α decreases significantly within the first $r \sim 5$ to $7 R_0$ but then remains approximately constant at larger radii. This demonstrates that for stable late-type stars there may be significant changes in α near the star where key observables such as polarization, continuum emission, and spectral lines are formed.

5. Discussion

Typical values of α considered for Be star disks fall in the range from 0.1–1.0 (for example, see Lee et al. 1991; Jones et al. 2008; Okazaki 2001). Recently, values of constant α through detailed modeling have been determined for particular Be stars. Carciofi et al. (2012) determined a value of $\alpha = 1.0 \pm 0.2$ for the disk of Be star, 28 CMa (ω Cma), by modeling the V-band excess during an episode of disk dissipation. Escolano et al. (2015), using spectroscopy analysis and a 2.5D disk oscillation model, found $\alpha = 0.8$ for the Be star, ζ Tau. Ghoreyshi & Carciofi (2017) were able to model the growth and dissipation phases with a constant α for the disk that varied with dissipation and growth cycles for ω Cma. They obtained values of α consistent with traditional values in the literature between 0.1 and 1.0. Interestingly, but perhaps not surprisingly, they found greater values of α for buildup phases compared to dissipation suggesting that for some stars the buildup is faster and perhaps more episodic than the dissipation phase. More recently, Rímulo et al. (2018) determined values of α for a set of 54 Be stars in the SMC using a semiautomatic pipeline to model their light curves. They obtained average values of α during buildup and dissipation of 0.63 and 0.26, respectively, for the set. It is important to note that their program stars were biased toward early types. Recently, as reported by Rímulo et al. (2018), Ghoreyshi & Carciofi (2017) revisited the value of α determined for ω Cma and obtained a smaller value of 0.21 ± 0.05 . Rímulo et al. (2018) explain that details of disk development over time must be considered to determine α due to a phenomena called the mass reservoir effect or the accumulation effect. Basically the length of time and the amount of material ejected into the disk ultimately affects the dissipation since some disks may accumulate a reservoir of material at large radial distances from the central star during the buildup phase or multiple buildup phases. In the case of a binary system the disk mass may build up inside the orbit of the secondary (see Panoglou et al. 2016; Cyr et al. 2017 for additional discussion). Potentially this effect may have led to an overestimate of α in some of the earlier work. Basically, when ejection of material into the disk stops or is reduced, if a large reservoir of material has built up, then it takes longer to empty the disk or requires a larger α . In a follow-up paper, Ghoreyshi & Carciofi (2018) analyzed the disk system for ω Cma and found much smaller values than the work of Carciofi

et al. (2012) by taking the history of the disk into account. Ghoreyshi & Carciofi (2018) obtained α of 0.20 ± 0.03 , 0.13 ± 0.01 , and 0.21 ± 0.05 for three dissipation phases for ω CMa indicating that α also varies with time. More recently, Ghoreyshi et al. (2021) applied a radially variable α to fit the equivalent width of the H α line for ω CMa and found a range of α between 0.25 and 0.35. In this work, a very large disk was assumed and the fact that any oblation from stellar radiation was not included means that these values are upper limits. This hints at the importance of the radial extent of the disk to obtain a correct value of α .

Marr et al. (2021) studied the complete loss of the disk for the early Be star, 66 Ophiuchi. They find a value of α of 0.4 in combination with an isothermal disk temperature of 60% of the stellar effective temperature. These authors experimented with a variable disk temperature and variable α but found the constant values were the best fit. Also, the outer bounds of the disk were examined and the best-fit models had a radial extent of $115 R_*$ for the H α emitting region. Interestingly, comparing to the formula of Krtićka et al. (2011) for the outer disk radius adopted in this work (see Section 2), an outer disk radius of $125 R_*$ is predicted, which is in remarkably good agreement.

We emphasize that in the discussions above, the studies are focused on early-type Be stars undergoing disk formation and dissipation events. Also many of these systems are quite variable likely due to nonconstant mass injection into the disk and in the case of 66 Oph, exhibit extreme variability since the star completely lost its disk.

In this study we focus on stable, late-type Be stars perhaps indicating that there has been a constant mass ejection rate from the star into the disk corresponding to a constant supply of angular momentum. In fact, for 1 Del the H α emission has remained virtually unchanged for decades as noted previously.

From the disk angular momentum loss rates from Geneva models and the typical assumption of a constant α throughout the disk, we find that in the range of masses corresponding to late Be star ($3\text{--}5 M_\odot$) and for typical densities and isothermal temperatures, the values of α around 0.3. When exploring the radially varying α for the isothermal model with $n = 3.5$, we recover the previous situation finding that α varies smoothly in the H α line forming region.

For a more realistic case including a self-consistent disk temperature, for the disk model that best fits the observations of the star 1 Del, the distribution of α seems to be quite nonconstant, in particular in the innermost part of the disk. But we note, as shown in Figure 6 that for smaller values of angular momentum loss, the change in α is much less significant.

Finally, it is interesting to compare our results for the density distribution for 1 Del with Figure 13 in Vieira et al. (2017) where they classify disks based on the value of n and ($\log \rho_0$) as dissipating, steady state, or forming. Our results for the density distribution for 1 Del would place this system as dissipating using their scheme. Clearly, this is not the case for 1 Del. As mentioned previously, 1 Del has been observed to be very stable over periods of decades. We note that the study of Vieira et al. (2017) favored early-type stars with $T_{\text{eff}} > 14,000$ K and they also considered isothermal disks. Late-type Be stars have cooler disks and seem to approach critical rotation more easily than early types. The central star is therefore strongly gravity darkened with cool equatorial regions and hotter poles. The




resulting disk structure is strongly nonisothermal with cool regions along the equatorial plane. However, the hot stellar polar regions keep the upper and mid disk ionized with radial distance producing the emission. This would, in turn, result in fairly constant density with radial distance producing the small values of n that we find for this very stable system. Interestingly, Granada et al. (2018) found a clear trend with spectral type for the allowed limits for n and ρ_0 in Be stars: larger base densities are allowed for smaller n for earlier spectral types, indicating that earlier spectral types can have more massive disks.

Martin et al. (2019) also studied the values of α using the same prescription used here, but focused mainly on accretion disks. They find that, for fully ionized disks, values for α are in the range of 0.2–0.3 and note that α is smaller (in some cases by orders of magnitude) when the disks are not fully ionized. They hypothesize that this gives support for MRI as a driving mechanism in viscous accretion disks. We also consider MRI as a driving mechanism (see Section 3.5) and interestingly find that for the models with the power-law density exponent $n < 3$, i.e., density distributions that fall more slowly with distance from the central star, we obtain estimates for α that are an order of magnitude smaller. We also obtain values of the magnetic field consistently less than 10 G for all the models considered, which potentially could explain the lack of detection of magnetic fields in Be stars. Martin et al. (2019) also discuss Be star disks and the fact that in these systems α seems to have higher values than in accretion disks, which is consistent with our findings, but they note that this trend needs more study. Martin et al. (2019) also explain that once the flow becomes transonic the driving mechanism must change. We note that Be stars have outflow speeds that are typically much less than the sound speed (Bjorkman & Carciofi 2005), which can provide clues to the driving mechanism in these systems.

In summary, in the present article, we find that assuming isothermal disks for late Be stars with constant α , mass dependent density at the base (ρ_0) as derived by Vieira et al. (2017), and angular momentum loss rates from Granada et al. (2013), leads to values of α close to 0.3. These values are between the values found during formation and dissipation phases by Rímulo et al. (2018). Interestingly, however, for the disk structure derived from H α and SED fitting for the late-type Be star 1 Del, we find that there seems to be a significant radial variation in α near the central star within approximately five stellar radii for typical values of angular momentum loss rates considered in the literature. If, however, the angular momentum loss rates are overestimated as has been suggested in the literature (see Rímulo et al. 2018), the value of α with radial distance could become much more constant for the systems studied here.

The authors would like to thank the anonymous referee, who helped improve the paper with thoughtful questions and comments. C.E.J. and T.A.A.S. wish to acknowledge support from The Natural Sciences and Engineering Research Council of Canada (NSERC). A.G. acknowledges the financial support received from the Agencia Nacional de Promocion Cientifica y Tecnologica of Argentina (PICT2017-3790), and from UNRN grant PI2020-40-B-890.

ORCID iDs

A. Granada  <https://orcid.org/0000-0002-7805-6333>
 C. E. Jones  <https://orcid.org/0000-0001-9900-1000>
 T. A. A. Sigut  <https://orcid.org/0000-0002-0803-8615>

References

- Abt, H. A. 2008, *ApJS*, **174**, 499
 Abt, H. A., & Morrell, N. I. 1995, *ApJS*, **99**, 135
 Balbus, S. A., & Hawley, J. F. 1991, *ApJ*, **376**, 214
 Bernacca, P. L., & Perinotto, M. 1970, *CoAsi*, **239**, 1
 Bjorkman, J. E., & Carciofi, A. C. 2005, in ASP Conf. Ser. 337, The Nature and Evolution of Disks Around Hot Stars, ed. R. Ignace & K. G. Gayley (San Francisco, CA: ASP), 75
 Carciofi, A. C. 2011, in IAU Symp. 272, ed. C. Neiner et al., 325
 Carciofi, A. C., & Bjorkman, J. E. 2006, *ApJ*, **639**, 1081
 Carciofi, A. C., Bjorkman, J. E., Otero, S. A., et al. 2012, *ApJL*, **744**, L15
 Cochetti, Y. R., Zorec, J., Cidale, L. S., et al. 2020, *A&A*, **634**, A18
 Cranmer, S. R. 2005, *ApJ*, **634**, 585
 Cyr, I. H., Jones, C. E., Panoglou, D., Carciofi, A. C., & Okazaki, A. T. 2017, *MNRAS*, **471**, 596
 de Almeida, E. S. G., Meilland, A., Domiciano de Souza, A., et al. 2020, *A&A*, **636**, A110
 Ekström, S., Georgy, C., Eggenberger, P., et al. 2012, *A&A*, **537**, A146
 Escolano, C., Carciofi, A. C., Okazaki, A. T., et al. 2015, *A&A*, **576**, A112
 Espinosa Lara, F., & Rieutord, M. 2011, *A&A*, **533**, A43
 Fitzpatrick, E. L. 1999, *PASP*, **111**, 63
 Georgy, C., Ekström, S., Granada, A., et al. 2013, *A&A*, **553**, A24
 Ghoreyshi, M. R., & Carciofi, A. C. 2017, in ASP Conf. Ser. 508, The Be Phenomenon: Forty Years of Studies, ed. A. Miroshnichenko, 323
 Ghoreyshi, M. R., Carciofi, A. C., Jones, C. E., et al. 2021, *ApJ*, **909**, 149
 Ghoreyshi, M. R., Carciofi, A. C., Rvmulo, L. R., et al. 2018, *MNRAS*, **479**, 2214
 Granada, A., Ekström, S., Georgy, C., et al. 2013, *A&A*, **553**, A25
 Granada, A., Jones, C. E., Sigut, T. A. A., et al. 2018, *AJ*, **155**, 50
 Gulliver, A. F. 1981, *ApJ*, **248**, 222
 Haubois, X., Mota, B. C., Carciofi, A. C., et al. 2014, *ApJ*, **785**, 12
 Hirata, R. 1995, *PASJ*, **47**, 195
 Huang, W., Gies, D. R., & McSwain, M. V. 2010, *ApJ*, **722**, 605
 Hubert, A. M., & Floquet, M. 1998, *A&A*, **335**, 565
 Iliev, L., & Kubát, J. 2013, *BlgAJ*, **19**, 3
 Jaschek, M., Slettebak, A., & Jaschek, C. 1981, *Be Star Newsletter*, **4**, 9
 Jones, C. E., Sigut, T. A. A., & Porter, J. M. 2008, *MNRAS*, **386**, 1922
 Kervella, P., Arenou, F., Mignard, F., & Thévenin, F. 2019, *A&A*, **623**, A72
 Klement, R., Carciofi, A. C., Rivinius, T., et al. 2017, *A&A*, **607**, C1
 Krtićka, J., Kurfürst, P., & Krtićková, I. 2015, *A&A*, **573**, A20
 Krtićka, J., Owocki, S. P., & Meynet, G. 2011, *A&A*, **527**, A84
 Kubát, J., Kubátová, B., Doležalová, B., Iliev, L., & Šlechta, M. 2016, *A&A*, **587**, A22
 Kurfürst, P., Feldmeier, A., & Krtićka, J. 2014, *A&A*, **569**, A23
 Kurfürst, P., Feldmeier, A., & Krtićka, J. 2017, *A&A*, **613**, A75
 Labadie-Bartz, J., Chojnowski, S. D., Whelan, D. G., et al. 2018, *AJ*, **155**, 53
 Lee, U., Osaki, Y., & Saio, H. 1991, *MNRAS*, **250**, 432
 Marlborough, J. M., & Cowley, A. P. 1974, *ApJ*, **187**, 99
 Marr, K. C., Jones, C. E., Carciofi, A. C., et al. 2021, *ApJ*, **912**, 76
 Martin, R. G., Nixon, C. J., Pringle, J. E., & Livio, M. 2019, *NewA*, **70**, 7
 McGill, M. A., Sigut, T. A. A., & Jones, C. E. 2011, *ApJ*, **743**, 111
 Merrill, P. W. 1952, *ApJ*, **115**, 42
 Millar, C. E., & Marlborough, J. M. 1998, *ApJ*, **494**, 715
 Miroshnichenko, A. S., Bjorkman, K. S., Morrison, N. D., et al. 2003, *A&A*, **408**, 305
 Okazaki, A. T. 2001, *PASJ*, **53**, 119
 Panoglou, D., Carciofi, A. C., Vieira, R. G., et al. 2016, *MNRAS*, **461**, 2616
 Pickles, A., & Depagne, É. 2010, *PASP*, **122**, 1437
 Porter, J. M., & Rivinius, T. 2003, *PASP*, **115**, 1153
 Pringle, J. E. 1981, *ARA&A*, **19**, 137
 Rímulo, L. R., Carciofi, A. C., Vieira, R. G., et al. 2018, *MNRAS*, **476**, 3555
 Rivinius, T., Carciofi, A. C., & Martayan, C. 2013, *A&ARv*, **21**, 69
 Royer, F., Grenier, S., Baylac, M.-O., Gómez, A. E., & Zorec, J. 2002, *A&A*, **393**, 897
 Shakura, N. I., & Sunyaev, R. A. 1973, *A&A*, **24**, 337
 Sigut, T. A. A. 2011, in IAU Symp., 272, ed. C. Neiner et al., 426
 Sigut, T. A. A., & Jones, C. E. 2007, *ApJ*, **668**, 481
 Sigut, T. A. A., McGill, M. A., & Jones, C. E. 2009, *ApJ*, **699**, 1973
 Sigut, T. A. A., Tycner, C., Jansen, B., & Zavala, R. T. 2015, *ApJ*, **814**, 159
 Silaj, J., Jones, C. E., Sigut, T. A. A., & Tycner, C. 2014, *ApJ*, **795**, 82
 Silaj, J., Jones, C. E., Tycner, C., Sigut, T. A. A., & Smith, A. D. 2010, *ApJS*, **187**, 228
 Slettebak, A. 1982, in IAU Symp. 98, Be Stars, ed. M. Jaschek & H.-G. Groth, 109
 Struve, O. 1931, *ApJ*, **73**, 94
 Uesugi, A., & Fukuda, I. 1970, Catalogue of rotational velocities of the stars
 Vieira, R. G., Carciofi, A. C., Bjorkman, J. E., et al. 2017, *MNRAS*, **464**, 3071
 Wade, G. A., Petit, V., Grunhut, J., & Neiner, C. 2014, arXiv:1411.6165
 Zorec, J., Frémat, Y., Martayan, C., Cidale, L. S., & Torres, A. F. 2007, in ASP Conf. Ser. 361, Active OB-Stars: Laboratories for Stellar and Circumstellar Physics, ed. A. T. Okazaki, S. P. Owocki, & S. Stefl (San Francisco, CA: ASP), 539